BRNO UNIVERSITY OF TECHNOLOGY
VYSOKÉ UČENÍ TECHNICKÉ V BRNĚ

FACULTY OF ELECTRICAL ENGINEERING AND COMMUNICATION
DEPARTMENT OF RADIO ELECTRONICS

FAKULTA ELEKTROTECHNIKY A KOMUNIKAČNÍCH TECHNOLOGIÍ
ÚSTAV RADIOELEKTRONIKY

PERFORATED DIELECTRICS AND HIGHER ORDER MODE DIELECTRIC RESONATOR ANTENNAS

PERFOROVANÁ DIELEKTRIKA A DIELEKTRICKÉ REZONÁTOROVÉ ANTÉNY S VYŠŠÍMI MÓDY

SHORT VERSION OF DOCTORAL THESIS

Author (Autor práce)
Ing. Michal Mrnka

Supervisor (Školitel)
Prof. Dr. Ing. Zbyněk Raida

Defence date (Datum obhajoby)
29.6.2017

Opponents (Oponenti)
Prof. Davor Bonefačić
Prof. Michal Mrozowski

KEYWORDS

dielectric resonator antenna, directive antenna, mutual coupling, higher-order mode, perforated dielectrics

KLÍČOVÁ SLOVA

dielektrická rezonátorová anténa, směrová anténa, vzájemní vazba, vyšší mód, perforovaná dielektrika

STORAGE PLACE

Research department, FEEC BUT, Technická 3058/10, 602 00 Brno

MÍSTO ULOŽENÍ PRÁCE

Vědecké oddělení, FEKT VUT v Brně, Technická 3058/10, 602 00 Brno

The research described in my thesis was performed in laboratories of the SIX Research Center, the registration number CZ.1.05/2.1.00/03.0072, the operational program Research and Development for Innovation.

© Michal Mrnka, 2017

Contents

1 Introduction **2**

2 State of the Art **3**
2.1 Dielectric Resonator Antennas . . . 3
2.2 Gain Enhancement of a Single Element DRA . . . 3
2.3 Mutual Coupling in DRA Arrays . . . 4
2.4 Perforated Dielectrics . . . 4

3 Objectives **6**

4 Enhanced Gain Higher-Order Mode Dielectric Resonator Antennas **7**
4.1 Rectangular Directive DRA . . . 7
4.1.1 Antenna Configurations . . . 8
4.1.2 Infinite Ground Plane DRAs . . . 8
4.1.3 Finite Ground Plane Effects . . . 10
4.1.4 Experimental Verification . . . 11
4.2 Cylindrical Directive DRA . . . 13

5 Mutual Coupling in Higher-Order Mode DRA Arrays **16**
5.1 Mutual Coupling Between Resonators Operating with TE_{113} and TE_{115} Mode 17
5.1.1 Coupling Between the Resonators in TE_{113} Mode . . . 17
5.1.2 Coupling Between the Resonators in TE_{115} Mode . . . 18
5.2 Mutual Coupling Between Rectangular Resonators Operating with TE_{133} Mode . . . 19
5.3 Summary . . . 20

6 Perforated Dielectrics **22**
6.1 Perforated Dielectrics . . . 22
6.1.1 Anisotropic Materials . . . 23
6.1.2 Determining Effective Relative Permittivity Tensor for Plane Waves 23
6.1.3 Results . . . 25
6.2 Surface Wave Propagation in Perforated Substrates . . . 26
6.2.1 Surface Waves on Dielectric Slabs . . . 26
6.2.2 Determining Effective Relative Permittivity from Unit Cell Analysis 27
6.2.3 Summary . . . 28

Conclusions **29**

References **31**

Curriculum Vitae **34**

Chapter 1

Introduction

The first dielectric resonator antenna (DRA), proposed by Long et. al. in 1980s, showed that the dielectric resonators, well known from microwave circuits, can in fact become very efficient antennas if properly excited.

To list the main advantages we can mention for example high radiation efficiency, compact size, ease of excitation and a relatively large impedance bandwidth when compared to other resonant antenna elements. Very important design parameter which influences all the properties of the DRA is the dielectric constant of the resonator. In the last decade new ceramic materials with very high ε_{r} (above 100) and with very low dielectric losses even deep in the millimeter wave regions became available. Very compact devices can be built from high dielectric constant materials; on the other hand their bandwidth is inversely proportional to the dielectric constant value. Hence the most compact designs often suffer from very narrowband operation bandwidth. Moreover, the fabrication process required for building the DRA is in general more complex compared to other elements such as microstrip antennas. Increased costs are thus result of the more complex fabrication if small volume manufacturing is in question. Nevertheless, in the high volume production the costs can be significantly reduced.

In the last 30 years, many properties of dielectric resonator antennas have been studied and understood. New techniques for increasing the bandwidth, introducing multiple resonances, minimizing the dimensions etc. have been proposed. If the higher gain of the antenna was required, it was necessary to use a DRA array with element number based on the desired gain. Only recently the gain increase of the single radiating element became of interest.

Chapter 2

State of the Art

The state of the art review in three main areas of the theses are given here, i.e. higher-order mode DRAs, mutual coupling in DRA arrays and perforated dielectrics.

2.1 Dielectric Resonator Antennas

Until 1980s the dielectric resonators with high quality factors Q had been used as circuit elements in microwave filters and oscillators designs only [1] but the utilization of the electromagnetic (EM) fields escaping the resonator was firstly proposed by Long. et. at in 1982 [2]. Ever since then, the interest of researchers in this type of the new antenna element has grown rapidly and the number of publications dedicated to the DRA field still grows annually.

A simple cylindrical DRA is in the majority of cases excited either with the transverse magnetic $TM_{01\delta}$ (also designated as TM_{011}) mode providing vertical electric dipole like radiation pattern or with the hybrid electromagnetic $HEM_{11\delta}$ (also known as HEM_{111}) mode which provides radiation pattern similar to the horizontally placed magnetic dipole [3]. Equivalent modes with analogous radiation patterns can be excited in the rectangular DRA.

2.2 Gain Enhancement of a Single Element DRA

A cylindrically shaped resonator, operating with the low-order hybrid electromagnetic mode $HEM_{11\delta}$ placed above a sufficiently large ground plane, is probably the most frequently used DRA configuration [2]. This mode generates a broadside radiation pattern with linear polarization and a gain of about 5 dBi.

Several approaches have been suggested to increase the gain of the DRAs. Arraying of single element DRAs [4] is probably the most versatile method in which the gain value can be directly controlled by the number of elements in the array. Nevertheless, increased size, complexity and costs of the resultant antenna are the main disadvantages.

Gain of a single element DRA can be increased by excitation of a higher-order radiating modes in a single dielectric resonator. This approach has already been adopted in both rectangular and cylindrical DRAs. Petosa and Thirakoune in [5] and [6] showed that a DRA based on higher-order TE_{113} and TE_{115} modes in a rectangular resonator can achieve gains of 8.2 dBi and 10.2 dBi, respectively. The structure operating in TE_{115} mode [6] required a maximum resonator dimension of about $1.1\lambda_0$ when built from dielectric material with relative permittivity $\varepsilon_r = 10$, where λ_0 is the free space wavelength. Guha

et al. [7, 8] managed to excite higher-order $HEM_{12\delta}$ mode in a cylindrical resonator by introducing an air-filled cavity in the ground plane below the resonator.

2.3 Mutual Coupling in DRA Arrays

In general, mutual coupling among array elements can be responsible for radiation pattern distortions as well as for gain reduction that cannot be predicted by array factor and pattern multiplication principle. Moreover, it can alter the input impedance of array elements and thus cause impedance mismatch at the element terminals. The coupling level is influenced by the properties of single elements (directivity, sidelobes etc.), feeding network and last, but not least, by the separation between neighboring elements.

Mutual coupling between two DRAs was studied for the first time in [9]. The authors theoretically derived the mutual impedances and calculated mutual coupling for two hemispherical dielectric resonators operating in broadside TE_{111} mode and fed by a probe. Since hemispherical DRA is the only shape for which analytical field solution exists, mutual coupling between rectangular and cylindrical DRAs has been studied only numerically and experimentally in numerous papers, where authors used either short current probe [10, 11] or more frequently an aperture [12, 13] for feeding the dielectric resonators. The results of the literature investigations can be roughly generalized as follows. The coupling in the H plane of the resonators is stronger, if the element spacing is smaller than approximately $0.5\lambda_0$. With increasing the spacing, the E-plane coupling becomes stronger as it decays with spacing more steadily. At spacing $0.5\lambda_0$ the transmission coefficient between two cylindrical aperture-fed dielectric resonators ($\varepsilon_r \approx 10$) is approximately about -12 dB in the E-plane and about -15 dB in the H-plane [12], [13], [14]. At spacing $1\lambda_0$ we can expect, for the same resonators, transmission coefficient of about -20 dB in the E-plane and about -30 dB in the H-plane [12, 13]. In case of probe-fed resonators [11] with separation distance $0.5\lambda_0$ the transmission between resonators in their E-plane is -11.4 dB and in the H-plane -15.5 dB according to [11]. At spacing $1\lambda_0$ the transmission coefficient decreases to -17.8 dB for E-plane and -28.0 dB for the H-plane.

2.4 Perforated Dielectrics

One of the main reasons why DRAs are not more widely used in design of (sub-)mm wave antennas and arrays is the complexity of fabrication and mechanical adjustment of individual elements on the correct positions. One of the potential solutions is to utilize perforations in classical microwave substrates.

The perforations in substrates as means of relative permittivity reduction were successfully used in microstrip antenna design [15] to suppress the surface wave propagation on thick dielectric substrates with large relative permittivities. The main negative effects of surface waves are gain reduction and ripples in radiation pattern due to diffraction of the energy at the substrate edges.

The same concept of using perforations to control the effective permittivity was deployed by Patrovsky and Wu in [16] and [17] for design of so-called Substrate Integrated Image Guide (SIIG).

In [18] authors proposed linearly tapered slot antennas for 30 GHz and 94 GHz bands on synthesized low permittivity substrate. To lower the permittivity, air perforations were used. Another interesting design was introduced by Patrovsky and Wu in [19]. In the paper, a planar dielectric rod antenna formed on the same layer with SIIG feeding [17]

was proposed for 94 GHz band. Another SIIG fed antenna array for 94 GHz band directly integrated on semiconductor wafer was presented in [20].

The perforated single element DR antenna was firstly described by Petosa, Ittipiboon and Thirakoune in [21]. The authors then extended the concept for larger two-dimensional array antennas in [22] and [3]. Comparison between performance of perforated DRA array and patch antenna array of the same size at frequency 24.5 GHz can be found in [23]. The DRA array provided about 1 dB higher gain and 22 % larger impedance bandwidth with the same number of array elements.

Another application in which perforated dielectrics are used is the area of reflectarrays and transmitarrays. In [24] wideband single dielectric layer transmitarray of perforations with varying period and size was described.

Vast area where air perforations are used to control electromagnetic properties of dielectric objects is radio optics and transformation optics. Designs of various dielectric lenses were described in e.g. [25–27]. In [25] and [26], the authors used single layer perforated dielectric material with different distribution of perforations.

Chapter 3

Objectives

Objective 1

Proposing an original directive DRA element based on the excitation of higher-order modes.

Radiation patterns of the potentially promising higher order modes will be examined and based on the field distributions, suitable mode (or combination of multiple modes) should be utilized to build a high gain DRA antenna element. From manufacturing point of view it is desirable that the element is simple shaped (cylinder, rectangular parallelepiped). Since the higher order modes mostly suffer from the narrowband operation, the techniques used for bandwidth enhancement of the conventional DRAs will be tested whether they can provide any bandwidth improvement of the high gain DRA element. If they can, the tradeoff between the impedance bandwidth and radiation properties will be found.

Objective 2

Research of mutual coupling between the higher-order mode DRA elements.

The mutual coupling between two cylindrical (rectangular) high-gain DRA elements will be examined numerically and experimentally and the attention will be focused on linearly polarized elements. The result will be a set of recommendations for minimum element spacing as well as the consideration of HO mode excitation as a mutual coupling reduction technique.

Objective 3

Research and description of anisotropic behavior of perforated dielectric substrates. The excitation of surface waves on such substrates and evaluation of possible DRA performance deterioration.

The perforated substrates are to be examined, first, as unbounded perforated dielectrics for which the components of the permittivity tensor will be derived. In this way, theoretical, polarization sensitive model of a homogenous equivalent model based on quasi-static approximation will be given. Such a model can better suit specific applications with different propagation directions. Secondly, the analysis will be extended to surface waves on grounded dielectric substrates and the effective relative permittivity determination for TE and TM cases. At last, we evaluate the deterioration of DRA performance designed and fabricated using air perforations. The effects of perforated dielectric layer surrounding the resonator on radiation patterns as well as on mutual coupling between antenna elements will be evaluated.

Chapter 4

Enhanced Gain Higher-Order Mode Dielectric Resonator Antennas

It has been described in the previous chapter that a suitable, higher order mode excited inside a dielectric resonator antenna can increase its directivity whereas keeping its radiation efficiency high. As a result, gain of the antenna is enhanced. The authors have previously worked only with modes that were described by increased index number in one direction of the resonator achieving maximum gains of up to 10 dBi [6]. We turn our attention to higher modes with larger index numbers in two directions, which inevitably makes the geometry of the antenna electrically larger.

Hybrid electromagnetic mode HEM_{133} of cylindrical dielectric resonator and transverse electric mode TE_{133} of rectangular resonators with square footprint are investigated numerically as well as experimentally. These two modes provide very similar radiation patterns with three main lobes and relatively high directivity. The level of two of the sidelobes can be significantly reduced by suitably designing the size of the ground plane as well as by introducing a small air gap between the resonator and its ground plane, redirecting more energy towards the broadside lobe. Since the size of the air gap turns out to be an important design parameter of our HO mode antennas, we deal with it in a separate section.

Since the DRAs are very interesting millimeter (and sub-millimeter) wave elements, we turn our attention to more advanced fabrication technique for resonator's manufacturing. We use Low Temperature Co-fired Ceramics with very low losses (LTCC) to build a resonator for 26 GHz antenna. In simulations, we compare antennas based on two different LTCC materials, one cheap and suitable for rather lower frequency regions and one more expensive but dedicated for utilization up to 100 GHz. The antenna based on mm-wave LTCC material is assembled and measured with extremely good agreement between simulation and experimental results which is caused by higher accuracy in shape control in LTCC process.

4.1 Rectangular Directive DRA

As it has been shown by Petosa et al. [6], the higher order TE modes (TE_{113} and TE_{115}) of rectangular resonators can provide more directive radiation patterns compared to the fundamental broadside radiating mode TE_{111}. Nevertheless, even the directivity of the fundamental mode can be enhanced by a factor up to 2 dB by decreasing the size of the ground plane and constructively utilizing the ground plane edge diffraction.

Very interesting can be the excitation of modes with two modal indexes larger than 1. In this way, we end up with resonators with larger footprint compared to modes described in [6]. In this section, we focus on TE_{133}, which, as it turns out provide directive radiation pattern. We examine its behavior above infinite as well as above finite ground plane. Furthermore, we conduct parametric study and find optimal dimensions maximizing the broadside gain.

4.1.1 Antenna Configurations

We start with resonators with square footprint, since this geometry has only two degrees of freedom: height h and width w. Size reduction in y direction follows resulting in antenna with rectangular footprint. With rectangular geometry, we can further suppress additional modes that are excited inside the square resonators. As the other modes help to increase impedance bandwidth quite significantly, the change of geometry to rectangular is used only to examine the characteristics of the isolated TE_{133} mode and to show, how the size of the antenna can be reduced if one sacrifices the impedance bandwidth.

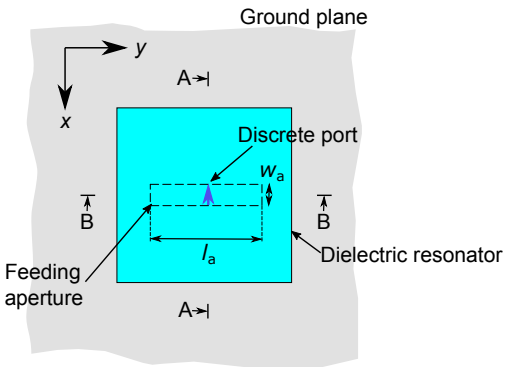

Fig. 4.1: Detail on the aperture feeding of the resonator. The input impedance of the discrete port in the simulations is set to 50 Ω

4.1.2 Infinite Ground Plane DRAs

Rectangular resonators have in general three degrees of freedom considering the design process, height h, width w and length d (see Fig. 4.8). In order to make the analysis systematic, we present characteristics in the following manner. We first select certain height of the resonator h between 11 and 15 mm. Then, using DWM we determine dimensions of a square footprint resonator ($w = d$) for resonant frequency $f_r \approx 10$ GHz. Afterwards, we fix the dimension w and we gradually change the length d from 5 mm up to $d = w$. For these dimensions, we examine input port reflection coefficient, maximum gain and radiation patterns in E and H planes. According to the Fig. 4.8, E-plane corresponds to the $phi = 0°$ and H-plane to $phi = 90°$. The resonator is fed by a centrally placed aperture with dimensions $l_a = 9$ mm and $w_a = 1.5$ mm and the aperture is excited by a discrete port with input impedance 50 Ω. The visualization of electromagnetic field components corresponding to the TE_{133} mode can be found in figures 4.2 to 4.3

For parametric study, we use simplified model of DRA above infinite ground plane with aperture, fed by a discrete port. The properties of the dielectric resonator are $\varepsilon_r = 6.15$ and $\tan\delta = 0.003$ corresponding to Arlon 600 substrate from which the resonators are be built in the following section. However, in this section we still consider the resonators to be built from single piece of dielectric material. The size of the ground plane (the distance

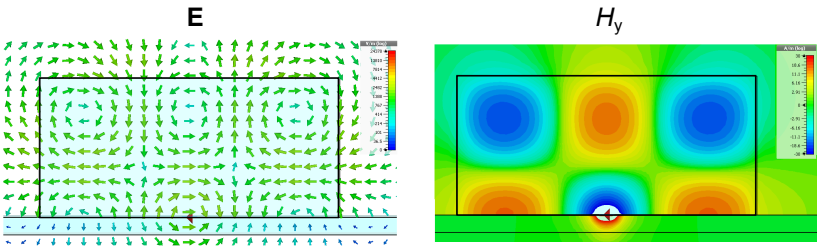

Fig. 4.2: Electric and magnetic fields in cross section A-A of the resonator (see Fig. 4.8)

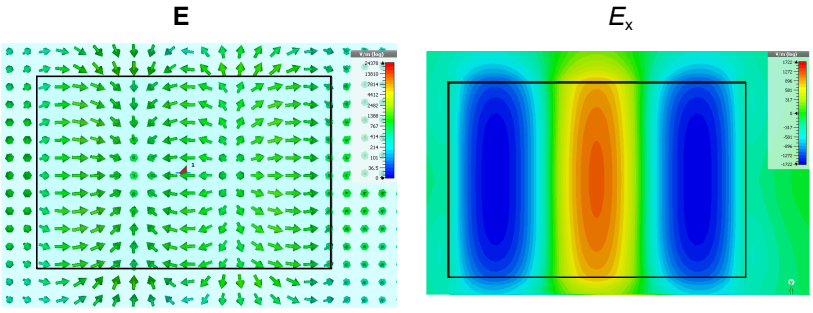

Fig. 4.3: Electric field distribution on the top wall of the resonator.

of PML boundaries from the resonator) must be chosen large enough not to influence the field distribution inside the resonator and the surface currents on the ground plane. In our simulations the size of the square ground plane is $g \approx 3\lambda_0$.

For h larger than circa 15 mm, TE_{115} and TE_{133} mode resonant frequencies are rather close and the radiation patterns of these modes cannot be separated. For this reason, we do not give any results for these dimensions. For larger h it is not possible to excite the desired TE_{133} mode efficiently.

The E-plane radiation patterns show three main lobes at $theta = 0\,°$, and $theta = \pm 90°$. For certain dimensions, another two sidelobes around angles $theta = \pm 45°$ arise. We can assume that the finite ground plane reduces the radiation towards $theta = \pm 90°$; however, radiation in these directions disqualify this element from 2D array applications (1D H-plane array should be possible as we show in chapter 5), where we cannot rely on edge diffraction between adjacent elements. However, additional structures could suppress the radiation in these directions.

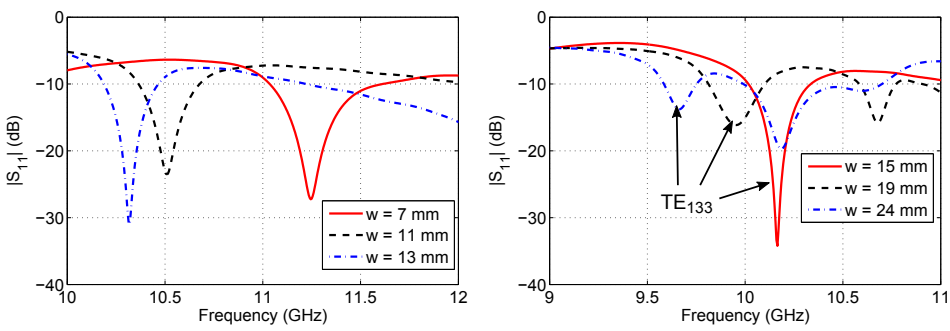

Fig. 4.4: Input port reflection coefficients showing resonances of TE_{133} mode $h = 13$ mm.

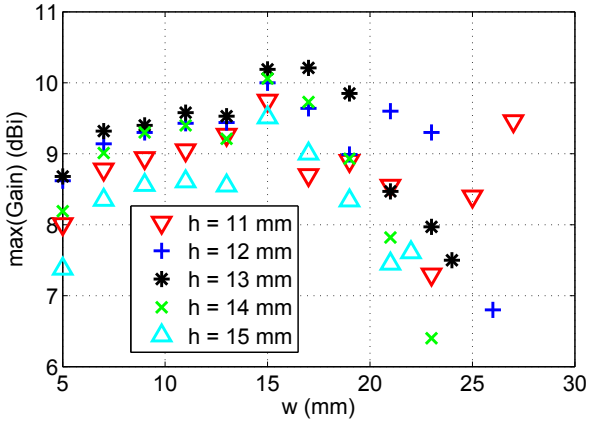

Fig. 4.5: Maximum gain corresponding to the TE_{133} mode as function of resonator's width w for various heights of the resonator.

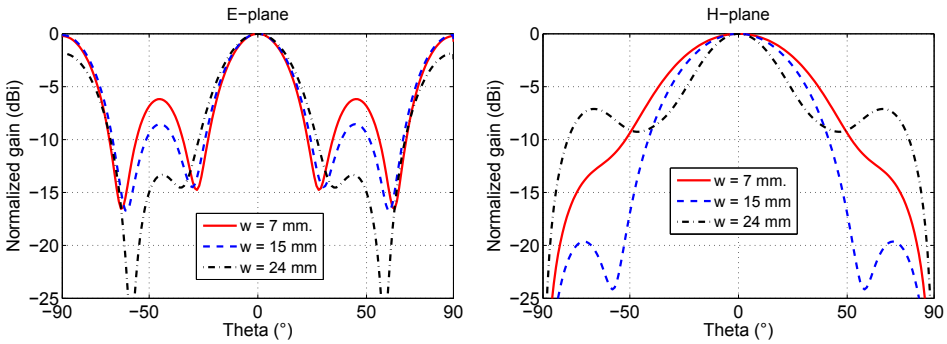

Fig. 4.6: Radiation patterns for resonator with height $h = 13$ mm and for various widths w. For frequencies see Fig. 4.4.

4.1.3 Finite Ground Plane Effects

It turns out that the size of the ground plane has a considerable effect on radiation patterns as well as on the maximum achievable gain in the broadside direction (i.e. $theta = 0°$, see Fig. 4.8). This gain variation can be explained by the edge diffraction in the E-plane (i.e. xz plane in Fig. 4.8) due to two beams at the angles $theta = \pm 90°$, i.e. in the reflector plane (see e.g. Fig. 4.6). The gain maximum in the broadside direction is obtained when the direct and diffracted waves meet in phase in direction $theta = 0°$.

In the simulation model, we choose square shape of the ground plane with side length g. We gradually increase g and we observe how the gain in the broadside direction varies as a function of g. For visualization, we express g in free space wavelengths λ_0. From Fig. 4.7 we can see, that the gain maxima (or minima) occur, whenever we increase g by approximately $2\lambda_0$ ($2\lambda_0$ is the period). The increase of g by $2\lambda_0$ corresponds to increase in distance between resonator's phase center and one of the edges by λ_0.

The DR has in this case dimensions $h = 13$ mm, $d = 24$ mm, $w = 17$ mm (i.e. resonator with maximum gain). Next, we show radiation patterns for several ground plane sizes, showing increasing ripples, especially in the E-plane. The reason is clearly the two beams directing towards ground plane edges in the E-plane. In the H-plane, there is only a little radiation towards the edges. As the diffraction causes propagation of waves also in the directions corresponding to lower half-space (contrary to the section 4.1.2 for infinite plane) we are now interested in radiation patterns in full range of angle $theta$: $-180° \leq theta \leq 180°$.

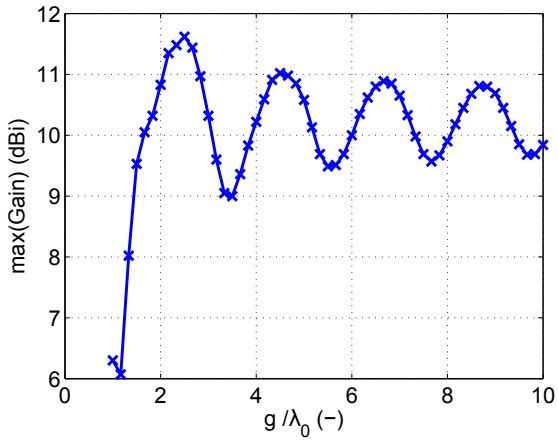

Fig. 4.7: Realized gain in direction $theta = 0°$ as a function of the ground plane size g at frequency 10 GHz. The period corresponds to approximately $2\lambda_0$.

4.1.4 Experimental Verification

In actual design, we work with a square footprint resonators and we excite dominantly TE_{133} mode of the resonator. However, as has been shown in previous sections, in square resonator, multiple modes can be excited and thus expand the impedance bandwidth of the antenna.

The antenna is configured as a rectangular dielectric resonator with a square footprint (i.e. width w and depth d are equal) above a conductive ground plane according to Fig. 4.8. The dielectric resonator is fed by an aperture coupling from a 50 Ω microstrip line. The relative permittivity of the resonator in the simulations is 6.15 and loss tangent tanδ = 0.003.

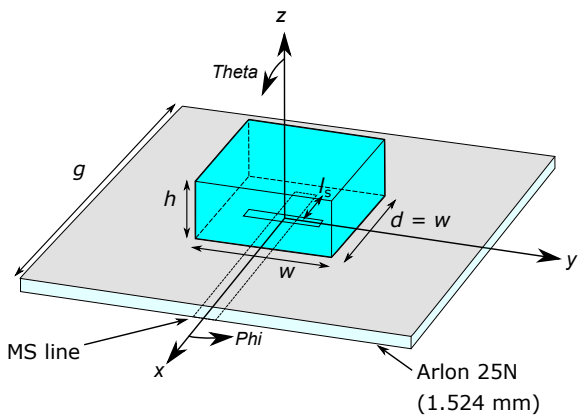

Fig. 4.8: Detail of the microstrip fed antenna.

We follow the design procedure outlined in the previous section and for the demonstration we select a center frequency 10.25 GHz. We are looking for the optimum aspect ratio to maximize the gain of the antenna. From this point of view, the optimum aspect ratio is found to be w/h = 26.4mm/11.3mm. In our case of the square footprint resonator, two additional resonances at both sides of the desired operating frequency occurs (most obvious are modes TE_{213} and TE_{115}), therefore increasing the impedance bandwidth significantly.

Throughout the thesis, the resonators are mostly build by a fabrication technique in which we layer up conventional microwave substrates. The antenna prototype is manufactured by assembling several layers of completely etched Arlon 600 substrate ($\varepsilon_r = 6.15$,

tanδ = 0.003) and the individual layers are held together by a special, double-sided duct tape with known electrical properties($\varepsilon_r \approx 3$). Due to the nature of the fabrication process, the height of the resonators must be an integer multiple of 1.575 mm (i.e. thickness of one layer of Arlon 600 substrate); in addition, the thickness of one layer of tape is about 50 μm, which also must be taken into account as it increases the overall height of the resonator. Considering these additional requirements, the resonator is slightly redesigned and its final dimensions are given in the Tab. 4.1.

Tab. 4.1: Final dimensions of the antenna.

h (mm)	w (mm)	l_a (mm)	g (mm)
11.38	26.75	13.10	77

The reflection coefficient frequency response is measured and the measured results of its magnitude are compared with simulation results of the redesigned resonator in Fig. 4.9. The differences might be explained by the absence of the SMA connector in the simulations but it is much more likely that the fabrication tolerances cause the discrepancy. The upshift of the resonant frequency can be explained by small amounts of air trapped between the adjacent resonators layers, which slightly decrease the effective permittivity of the resonator.

The realized gain is measured at several frequencies and the results are given in Fig. 4.10. The enhanced gain region at the target frequency 10.25 GHz is therefore confirmed with maximum value 11.9 dBi. Normalized radiation patterns in principal planes of the antenna are given in Fig. 4.11.

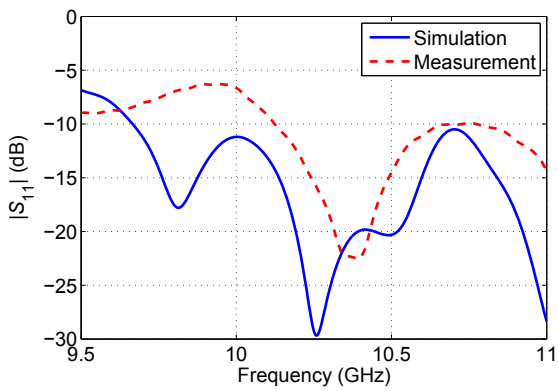

Fig. 4.9: Comparison between simulated and measured reflection coefficient. The measured results varied from simulated due to inaccurate fabrication.

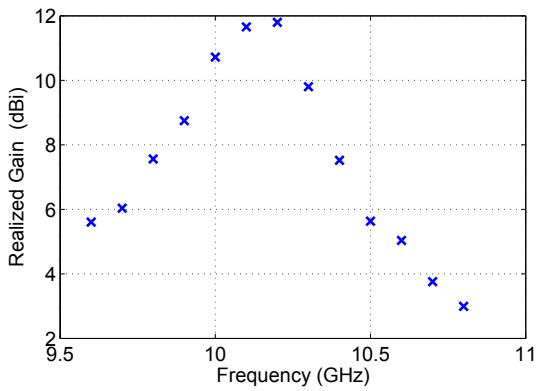

Fig. 4.10: Realized gain frequency response. Maximum achieved gain is 11.9 dBi.

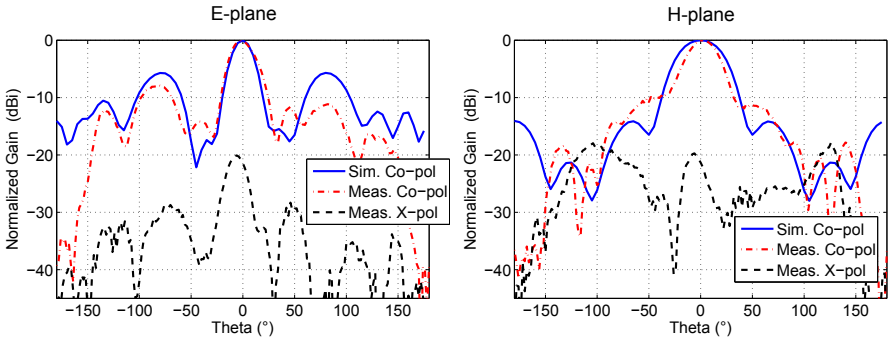

Fig. 4.11: Normalized radiation patterns in both principal planes (E-plane on the left, H-plane on the right).

4.2 Cylindrical Directive DRA

Similar effects as accomplished with the TE_{133} mode of rectangula resonators can be obtained if the cylindrical resonator operates with a hybrid HEM_{133} mode. We observe partial excitation of the nearby HEM_{123} mode which slightly increase the gain, but more visibly the impedance bandwidth of the antenna. Similarly to conventional DRAs, where broadside radiating modes TE_{111} of rectangular and HEM_{111} of cylindrical resonator show very similar characteristics we can assume that HEM_{133} mode will resemble in performance the TE_{133} mode of rectangular resonator. Compared to rectangular resonator, the analysis and design of cylindrical resonators is more straightforward as the cylinders possess only two degrees of freedom (i.e. height and diameter) for selected relative permittivity.

A parametric study in CST Microwave Studio is conducted to observe the behavior and to determine the limits of the proposed DRA at the center frequency 5.8 GHz. We focus on various diameter to height ratios (aspect ratio) as well as on ground plane size, which, as in case of rectangular DRA operating with TE_{133} mode has noticeable effect on the E-plane radiation patterns as well as on the broadside gain values.

The antenna is composed of a single cylindrical dielectric resonator placed above a circular conductive ground plane. The resonator is excited through a rectangular slot in the ground plane of a microstrip line according to Fig. 4.12. An aperture coupling feeding mechanism is selected to minimize excitation of unwanted lower-order modes in the structure. Relative permittivity of the resonator in all simulations is 6.15. The substrate Arlon 25N with relative permittivity 3.38 is used in the feeding structure design.

The design procedure again follows the procedure outlined for the rectangular DRA.

We are looking for optimum height/diameter ratio that maximizes the gain in the broadside direction.

The E-field oscillates predominantly in the x-axis direction(y-field components are symmetrical and thus cancel each other out) and thus the radiation is linearly polarized in the broadside direction (the direction along the z-axis). A relatively high gain radiator with radiation efficiency above 90 % can be obtained by carefully optimizing the resonator's size, dimensions of the aperture feed and the ground plane diameter.

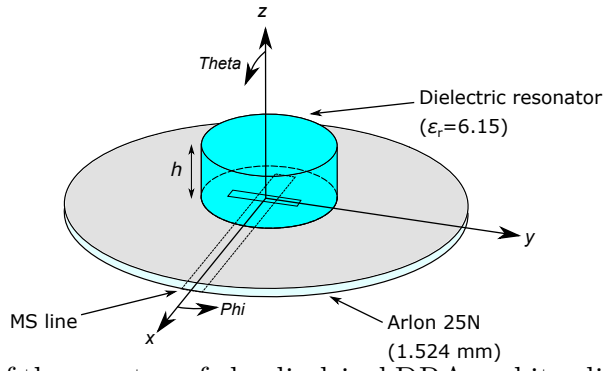

Fig. 4.12: Geometry of the aperture-fed cylindrical DRA and its alignment in the spherical coordinate system.

Due to the restrictions of the antenna fabrication method, the height h must be an integral multiple of 1.575 mm only, which is the height of the Arlon substrate used for manufacturing. The optimum height h, providing the maximum gain is found to be 22.05 mm corresponding to 14 layers of the Arlon substrate. The desired resonant frequency was 5.8 GHz with the band of interest covering the frequency range 5.725-5.875 GHz (ISM band). The band of interest corresponds to a relative bandwidth of only 2.6 %. Throughout the parametric study, the dimensions of the feeding structure (i.e. the slot width w_a, its length l_a and the stub length l_s) are kept constant as well as the height h of the resonator.

The resonant frequency of the DRA and its impedance bandwidth are determined mostly by the dimensions of the resonator whereas its gain is in addition quite strongly influenced by the diameter of the ground plane.

The antenna is fabricated by the same process as described for rectangular resonator case. Due to this fact, the dimensions of the anetnna must be slightly tuned by altering the resonator diameter to compensate for the effect of 14 layers of the duct tape in between the dielectric layers. The final dimensions of the resonator are $h = 22.75$ mm corresponding to 14 layers of Arlon 600 substrate interleaved with 14 layers of duct tape. The diameter of the resonator is 44.1 mm and the diameter of the ground plane $g = 132.5$ mm.

The comparison between the simulated and measured magnitude of the reflection coefficient is depicted in Fig. 4.13; reasonable agreement can be observed. The gain frequency respopnse comparing simulation and measurement results is given in Fig. 4.14. The maximum measured gain 11.59 dBi occurs at the frequency 5.82 GHz. The sidelobe level is -8 dB (critical is the E-plane) and the cross-polar discrimination 20 dB.

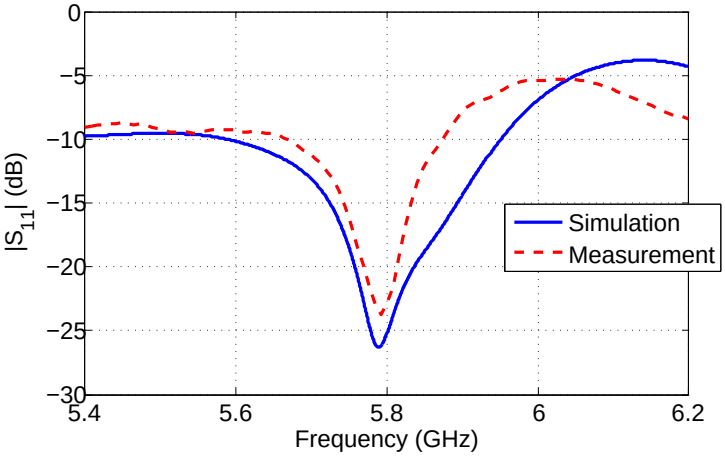

Fig. 4.13: Comparison between simulated and measured reflection coefficient.

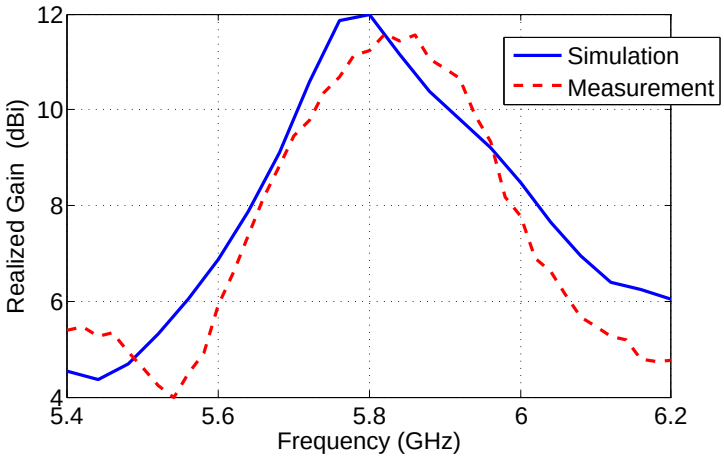

Fig. 4.14: Realized gain frequency response in the broadside direction.

Chapter 5

Mutual Coupling in Higher-Order Mode DRA Arrays

In this chapter, mutual coupling between two dielectric resonators is examined. Focus is drawn to resonators operating in higher-order modes for gain enhancement of single element dielectric resonator antennas. The modes comprise TE_{113} ($TE_{\delta 13}$) and TE_{115} ($TE_{\delta 15}$) of rectangular resonator, whose enhanced gain was described by Petosa et al. [5, 6] and mode proposed in this theses, i.e. TE_{133} [28] of rectangular resonator.

The problem is analyzed numerically and experimentally. The common approach to investigate the level of mutual coupling in antenna array is to analyze the interaction between only two elements. Two geometrical configurations of elements are taken into account. First, the elements are located next to each other so that the E-planes of the elements coincide (see Fig. 5.1). And second, the elements are placed so that their H-planes coincide (Fig. 5.2).

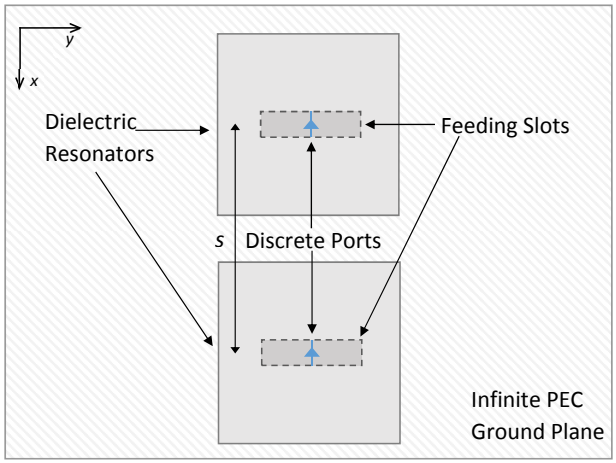

Fig. 5.1: Configuration of two aperture-fed dielectric resonators for analyzing coupling in the E-plane of the resonators (top view).

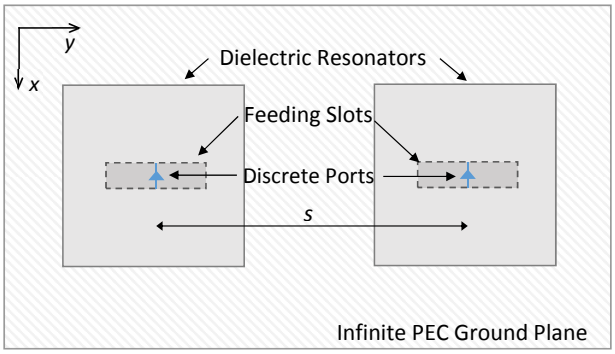

Fig. 5.2: Configuration of two aperture-fed dielectric resonators for analyzing coupling in the H-plane of the resonators (top view).

5.1 Mutual Coupling Between Resonators Operating with TE_{113} and TE_{115} Mode

The directive radiation patterns of these modes were described by Petosa et al. in [5, 6]. For design, the authors used materials with relative permittivity of $\varepsilon_r \approx 10$ and obtained broadside radiation patters at 11 GHz with maximum gains 8.2 and 10.2 dBi with excitation of TE_{113} and TE_{115}, respectively. We analyze the mutual coupling between two identical resonators operating either with TE_{113} or TE_{115} mode. The outcomes of the analysis are supposed to give general hints for antenna array design, as we believe these elements are very promising in antenna array applications.

In the analysis of mutual coupling, we first design isolated elements operating with TE_{113} and TE_{115} modes having aspect ratios that provide maximum gain (fields are given in Fig. 5.3). The simulation model is in this phase as simple as possible – resonator is placed on top of an infinite PEC ground plane and fed by a discrete port (Fig. 5.1).

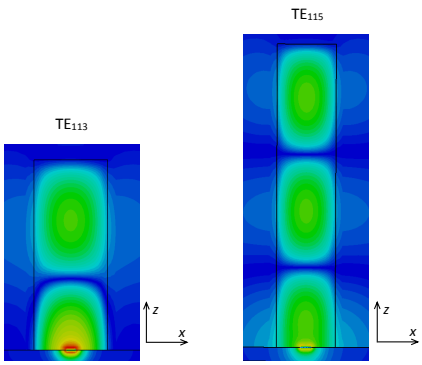

Fig. 5.3: H_y magnetic field component in the cross-section of the resonator.

5.1.1 Coupling Between the Resonators in TE_{113} Mode

The E-plane and H-plane arrangements of the resonators as given in Fig. 5.1 and Fig. 5.2 are used to determine the coupling level in between the two identical resonators operating with TE_{113} mode. However, small amount of coupling might be present in case of discrete port feeding due to surface waves in Arlon 25N substrate. The transmission coefficient between the slots is only-40 dB in the E-plane and -47 dB in the H-plane.

We proceed to simulations of two resonators as designed before, the footprint of the resonators is of size w x w = 6.35 mm x 6.35 mm. Therefore, the minimum spacing s is

selected to be $s = 6.5$ mm in the E-plane as well as in the H-plane. The spacing is varied from $s = 6.5$ mm up to 50 mm, what corresponds to electrical lengths $0.2\lambda_0 - 1.55\lambda_0$ at the 9.2 GHz resonant frequency. The transmission coefficient between the resonators S_{21} as a function of s is shown in Fig. 5.4.

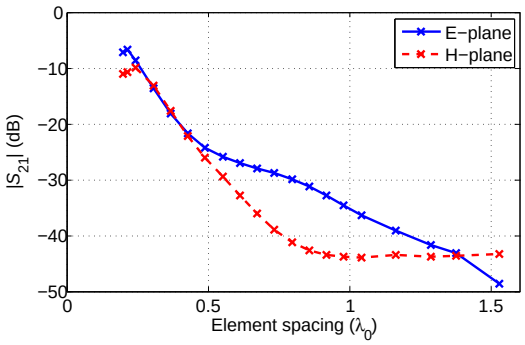

Fig. 5.4: Transmission coefficient as a function of element spacing in both principal planes for TE_{113} mode ($f = 9.2$ GHz).

5.1.2 Coupling Between the Resonators in TE_{115} Mode

The same simulation approach as deployed in the previous section is used here to evaluate the coupling levels between two identical resonators operating in TE_{115} mode. Transmission coefficient in both principal planes as functions of inter element spacing s are given in Fig. 5.5.

The presence of larger side lobes in radiation patterns in H and E plane – assuming stronger coupling, as well we can assume stronger E plane coupling. Coupling reduction capability of this mode is thus not that efficient as with TE_{113} mode.

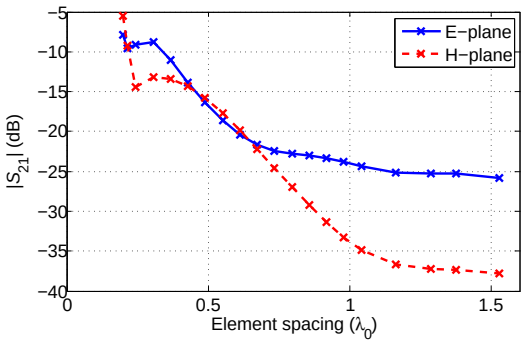

Fig. 5.5: Transmission coefficient as a function of element spacing in both principal planes for TE_{115} mode ($f = 9$ GHz).

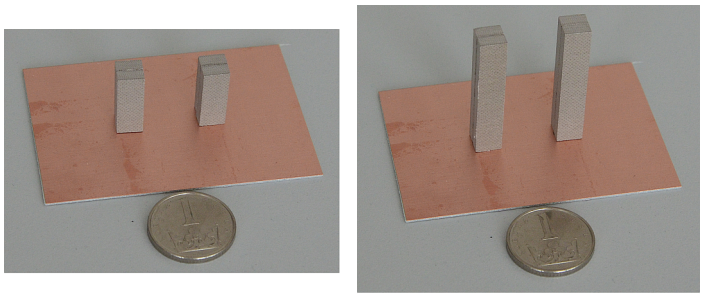

Fig. 5.6: Fabricated antennas operating with TE_{113} mode (left) and TE_{115} mode (right). The spacing between the antennas is in both cases $0.5\lambda_0$. The ground planes are identical.

5.2 Mutual Coupling Between Rectangular Resonators Operating with TE_{133} Mode

Finally, we evaluate mutual coupling between the resonators described in chapter 4. We use modified resonators with rectangular footprint. In section 4.1 it was shown, that if we do not want to excite multiple modes and thus create multiple coupling channels we should carefully design the dimensions of the resonator. The resonators are designed according to the chapter 4 for 9.3 GHz resonant frequency.

Once the single element model is prepared and its characteristics evaluated, two resonators operating with TE_{133} mode are aligned in their E- and H-planes according to the Fig. 5.1 and Fig. 5.2 and fed by discrete ports with input port impedance of 50 Ω. Transmission coefficient is evaluated for inter-element separation distances $s = 0.4\lambda_0$ to $1.55\lambda_0$ in the H-plane and $s = 0.87\lambda_0$ to $s = 1.55\lambda_0$ in the E-plane. The reason why the separation distance in the E-plane does not start with a smaller value is caused by physical dimensions of the resonators, as it is impossible to achieve smaller s than about $s = 0.84\lambda_0$, at this value there is a connection between the walls of the resonators.

The large value of mutual coupling (i.e. -7.7 dB) in the E-plane at separation distance $1\lambda_0$ (Fig. 5.7) and the size restrictions suggest, the elements operating in TE_{133} mode are simply not suitable for arraying along their E-plane. Other techniques (e.g. finite ground plane, EBG structures for ground plane etc.) might be used to limit the sidelobe levels and increase the directivity in this plane. On the other hand, the dimensions and mutual coupling performance in the H-plane (Fig. 5.7) prove the possibility to use these elements for H-plane linear arrays.

In field simulations without the interleaved glue layers present, the resonant frequency is approximately 9.3 GHz; however, measured value is little higher 9.5 GHz. Lower relative

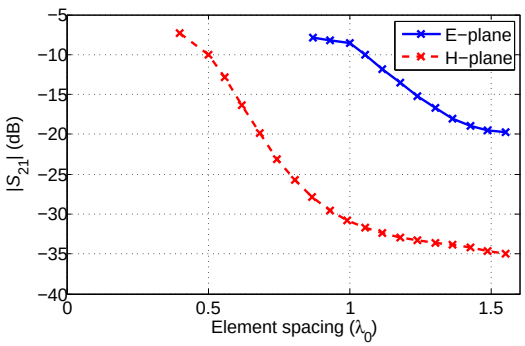

Fig. 5.7: Transmission coefficient as a function of element spacing in both principal planes for TE_{133} mode at 9.3 GHz.

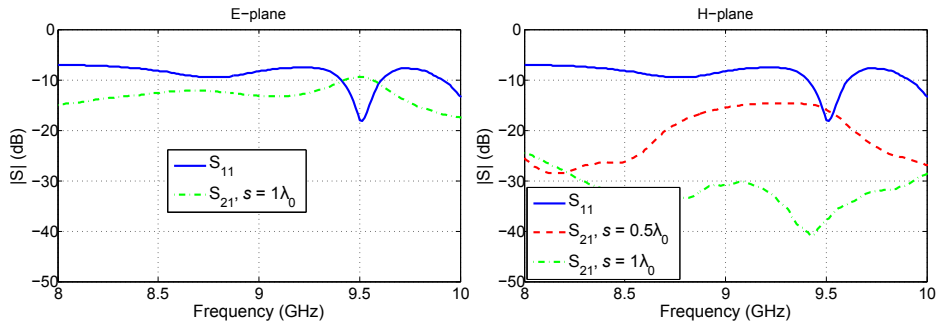

Fig. 5.8: Frequency response of reflection and transmission coefficient magnitude in the E-plane (left) and in the H-plane (right) of the resonators operating with TE_{133} mode.

permittivity and the air gaps between the layers of the resonator (9 layers in total for each resonator) cause the effective permittivity of the resonator to be somewhat lower than expected 6.15 of Arlon 600. As a result, the resonant frequency slightly rise. This frequency change correspond to relative frequency shift of 2.1 %.

5.3 Summary

In our analysis, dielectric resonators operating with higher-order modes TE_{113} and TE_{115} turn out to be suitable elements for antenna array applications. According to simulations and measurements, both modes TE_{113} and TE_{115} are capable of decreasing the mutual coupling between the dielectric resonators in the E-plane as well as in the H-plane. The excitation of HO mode can thus be considered as an mutual coupling reduction technique. The obvious advantage is that there is no need for additional elements between or in the vicinity of the antennas [29]. The most important results are summed up in tables 5.1 and 5.2.

Due to considerably larger size of the TE_{133} mode resonators (larger footprint) and due to the large sidelobes in the E-plane, the coupling is stronger in this plane than in case of the fundamental TE_{111} mode. In the H-plane, the values are very similar to the fundamental mode DRA. For this reason, TE_{133} is not suitable for coupling reduction; however, it can still be used for one dimensional H-plane antenna arrays design with similar amounts of coupling among the elements as in case of TE_{111} mode antennas (see Tab. 5.3).

Tab. 5.1: Results of measurement and simulation of transmission coefficient between two resonators operating with HO modes, i.e. TE_{113}.

	$\lvert S_{21}\rvert$ [-]							
Plane	E-plane				H-plane			
s [λ_0]	0.58		1.16		0.58		1.16	
Meas./Sim.	M	S	M	S	M	S	M	S
TE_{113}	-27.3	-26.5	-39.4	-39.14	-27.4	-30	-41	-43.4

Tab. 5.2: Results of measurement and simulation of transmission coefficient between two resonators operating with HO modes, i.e. TE_{115}.

	$\|S_{21}\|$ [-]							
Plane	E-plane				H-plane			
s [λ_0]	0.56		1.12		0.56		1.12	
Meas./Sim.	M	S	M	S	M	S	M	S
TE_{115}	-21.4	-19.0	-26.0	-24.9	-17.7	-18.2	-34.1	-35.5

Tab. 5.3: Results of measurement and simulation of transmission coefficient between two resonators operating with HO modes, i.e. TE_{133}.

	$\|S_{21}\|$ [-]							
Plane	E-plane				H-plane			
s [λ_0]	0.5		1		0.5		1	
Meas./Sim.	M	S	M	S	M	S	M	S
TE_{133}	-	-	-9.4	-8	-15.9	-10	-35.7	-31
TE_{111}	-13.3	-12.9	-19.1	-19.2	-	-	-	-

Chapter 6

Perforated Dielectrics

As indicated in chapter 2, one of the main reasons why DRAs are not more widely used in the design of (sub-)mm wave antennas and arrays is the complexity of fabrication and mechanical adjustment of individual elements on the correct positions. Perforated dielectric structures can deal with this problem. However, in this as well as in other applications reviewed in section 2.4, the problem of effective relative permittivity calculation arise. In the open literature, the available formulas do not respect the anisotropic nature of perforated dielectric layers. The main focus of this chapter is therefore on the development of analytical model of perforated material capable to describe anisotropic properties for transverse electromagnetic waves as well as for surface waves propagating on perforated dielectric slabs.

6.1 Perforated Dielectrics

From physical point of view, the perforated dielectric layers (substrates) are through-hole porous materials in which perforations (pores) operate in sub-wavelength regime in which it follows that the wavelength is much larger than the period of perforations (except of the EBG applications).

Porous materials are created by embedding pores (in our case through hole perforations) into a matrix medium (dielectric substrate in our case), thus forming a heterogeneous media of at least two constituents. The pores can have various shapes and sizes including complex fractal shapes. It follows that in certain cases the porous media can have anisotropic properties.

The theoretical foundation upon which the theory of porous dielectrics, in fact the theory of all dielectric mixtures, is based on the Lorenz internal field theory [30].

By applying the famous Maxwell Garnett (MG) mixing rule to the goemetry of the perforated dielectric layer we can find out the relative permittivities depending on the direction of the electric field vector. In the direction of optical axis, the perforations are unbounded, however, in the plane perpendicular to the optical axis the perforations are bounded.

In case of electric field perpendicular to the optical axis, the depolarization factor $N = 1/2$ and the effective permittivity is given as:

$$\varepsilon_{\text{eff}} = \varepsilon + 2f\varepsilon \frac{\varepsilon_{\text{i}} - \varepsilon}{\varepsilon_{\text{i}} + \varepsilon - f\left(\varepsilon_{\text{i}} - \varepsilon\right)}, \tag{6.1}$$

where ε_{i} is the permittivity of the inclusions, which in case of air perforations is $\varepsilon_{\text{i}} = \varepsilon_0$ and f denotes crucial parameter of the porous materials called *porosity* or simply a volume fraction. The porosity lies between 0 and 1 and is often given in percent.

Considering polarization parallel to the axis of perforations, the depolarization factor is $N = 0$ (there are actually no bounded pores in this case) and thus the effective permittivity [31] is determined:

$$\varepsilon_{\text{eff}} = f\varepsilon_{\text{i}} + (1 - f)\,\varepsilon. \tag{6.2}$$

Our theoretical model of anisotropic perforated dielectric for TEM waves in unbounded space is therefore based on the equations 6.1 and 6.2 which were derived for the quasi-static approximation.

6.1.1 Anisotropic Materials

In the previous section, it has been shown that the effective permittivity of the perforated dielectric slab depends on the **E** field direction which makes the structure anisotropic (electrically anisotropic [32]). In anisotropic materials, the relation between **E** and **D** is no longer given by a scalar ε, but by a permittivity tensor $\overleftrightarrow{\varepsilon}$

$$\mathbf{D} = \overleftrightarrow{\varepsilon}\,\mathbf{E}, \tag{6.3}$$

The permittivity tensor is diagonalizable by suitable selection of the coordinate system (i.e. rotation of the permittivity matrix). In this new coordinate system, the axes are called principal axes and for the uniaxial media we can write the permittivity tensor in a form:

$$\overleftrightarrow{\varepsilon} = \begin{pmatrix} \varepsilon_o & 0 & 0 \\ 0 & \varepsilon_o & 0 \\ 0 & 0 & \varepsilon_e \end{pmatrix}. \tag{6.4}$$

By performing several numerical simulations on some test geometry of perforated dielectric material we can prove the material to be uniaxial.

6.1.2 Determining Effective Relative Permittivity Tensor for Plane Waves

There are many techniques to determine effective relative permittivity. In the numerical simulations we mostly work by determining the phase constant and by knowing the exact dimensions of the simulation model, we can simply calculate the effective permittivity. However, for the evaluation of dispersion diagrams and afterwards for calculation of effective relative permittivities we use unit cell analysis based on periodic boundary conditions.

The perforated material can also be analyzed as a periodic structure, in which the unit cell is repeated in one or two dimensions indefinitely using periodic boundary conditions and Floquet theory. Full material characterization under these conditions requires only the analysis of a single unit cell. Even though the structure can be described by triangular grid with periodicity p, for our purpose the unit cell must be formed as a rectangle with two periodicities: p_x designates the periodicity in the x-direction and p_y periodicity in the y-direction (Fig.6.1). The extraordinary axis of the material is aligned with z – axis of the coordinate system.

From unit cell figure (Fig. 6.1) we can see that

$$p_y = p, \tag{6.5}$$

$$p_x = p\sqrt{3}. \tag{6.6}$$

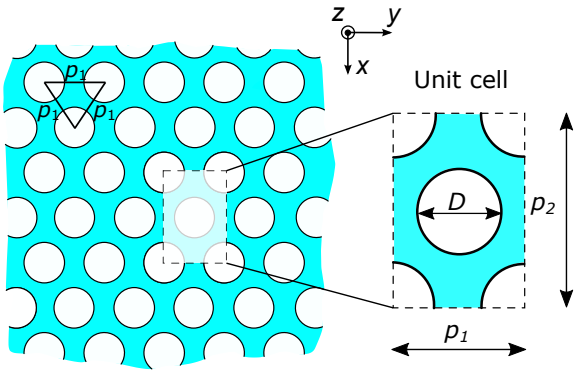

Fig. 6.1: Triangular lattice and the unit cell detail

Using modal analysis in CST Eigenmode solver we determine the dispersion diagrams of the unit cell for three electric field vector orientations (along the unit vectors). In case of **E** aligned parallel with x-axis, we set top and bottom boundary condition to be PEC (Perfect Electric Conductors) and all four side walls are periodic boundary conditions. On periodic walls, perpendicular to y-axis we set zero phase difference (magnetic walls can be used for this polarization as well) and on the walls, perpendicular to z-axis we gradually set values from 0° to 180°. The results are eigenfrequencies corresponding to these phase shifts.

This analysis is performed for three different values of period p ($p = 0.8$ mm $p = 1.5$ mm, 3 mm) and for each period, three different diameters of perforations are considered, $D = p/2$, $D = 2p/3$, $D = 5p/6$ and $D = p$. For example, for period $p = 3$ mm, the perforation diameters are 1.5, 2, 2.5 and 3 mm. It should be mentioned that the case in which $D = p$ is only theoretical and cannot be achieved in practical application, since the structure would lose its mechanical robustness. The exact values of the periods and diameters of perforations are selected to be approximately $\lambda_0/10$, $\lambda_0/20$ and $\lambda_0/37.5$ at frequency 10 GHz, with free space wavelength 30 mm.

Unit cell analysis does not allow us to receive attenuation constant of the material, only the phase constant can be obtained by considering total phase change over one meter. Knowing the phase difference over one unit cell $\Delta phase$ and the length of the unit cell l in the direction in which phase difference of $\Delta phase$ is applied, we can get the phase constant at calculated eigenfrequency as:

$$\beta = \frac{\Delta phase}{l}. \tag{6.7}$$

In this way, we repeat the simulations for TEM waves propagating in directions of axes x, y, z (principal axes) with two states of polarizations with respect to the structure geometry (if possible), i.e. electric field vector **E** parallel to the axis of cylindrical perforations and **E** perpendicular to the axis of perforations.

From theory, it follows that the propagation constant of a wave in anisotropic medium is determined by its polarization state with respect to the material's principal axes of anisotropy. In our situation, it means the propagation constant for TEM wave propagating in $\pm y$ direction is proved to be the same as the propagation constant of waves propagating in $\pm x$ or $\pm z$ directions with the **E** field oriented perpendicular to the axis of perforations. The simulation results also show that the propagation constant in x and y directions are the same making the media uniaxial, despite the triangular lattice. This holds true for both polarization states (**E** perpendicular and parallel to the axis of perforations). It means that the exact arrangement of the perforations is not relevant to the material

properties and the same results, from the qualitative point of view would, be acquired in case of different lattices, e.g. square, honeycomb etc. In terms of uniaxial media, we call the axis of perforations (z axis in Fig. 6.1) extraordinary axis and the axes x and z ordinary axes. It should be noted that this holds true only in the sub-wavelength regime of the perforations.

The propagation constants at calculated eigenfrequencies are then used to evaluate equivalent effective relative permittivity tensor of homogenized dielectrics (eq. 6.4).

$$\beta = \frac{2\pi}{\lambda} = \frac{2\pi\sqrt{\varepsilon_{\mathrm{r,eff}}}}{\lambda_0}, \tag{6.8}$$

$$\varepsilon_{\mathrm{r,eff}} = \frac{\beta^2\lambda_0^2}{4\pi^2}, \tag{6.9}$$

where β is the phase constant, λ is the wavelength in homogenized perforated dielectric, λ_0 is the free space wavelength and $\varepsilon_{\mathrm{r,eff}}$ is the effective relative permittivity of the homogenized perforated dielectric.

At higher frequencies, where the size of the period and perforations is closer to the wavelength, the material behaves as an Electromagnetic Band Gap structure. On top of the material dispersion of perforated dielectrics, the structure shows also waveguide dispersion and there is no sense in evaluation of the effective relative permittivity without taking waveguide dispersion into consideration. Due to our application, we decided to focus on dimensions that did not show bandgap behavior (i.e. sufficient number of perforations per wavelength) and where material homogenization can be utilized without any additional effects.

6.1.3 Results

The absolute dimensions of the single perforations are not that important if we operate the structure at wavelengths much smaller than the period of perforations. Under this condition, the permittivity is controlled only by the D/p ratio (i.e. porosity f). The comparison between results of theoretical model based on Maxwell-Garnett mixing rules (eq. 6.1 and 6.2) and numerical simulations for period of perforations $p = 0.8$ mm is given in Fig. 6.2. The agreement at lower frequencies (10 GHz), where $p = \lambda_0/37.5$ is excellent, in addition, the theoretical model seems quite accurate even at 40 GHz, where $p = \lambda_0/9.4$.

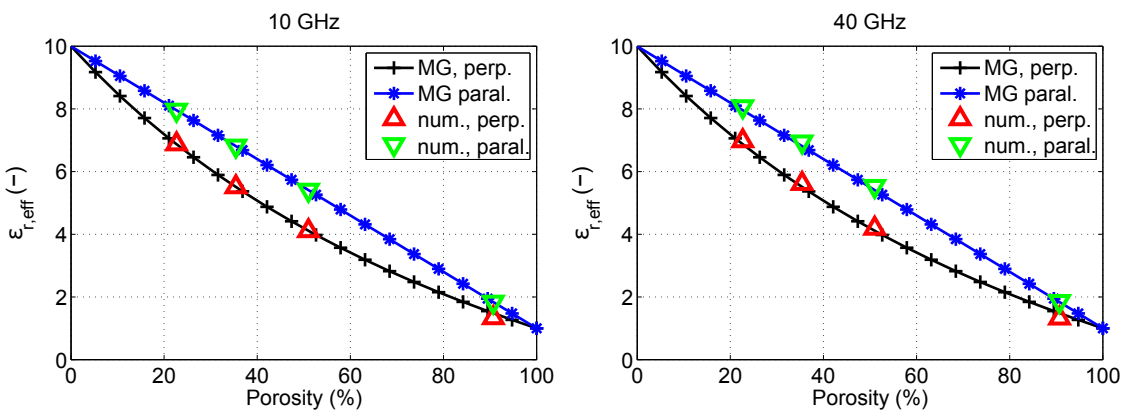

Fig. 6.2: Comparison between theoretical model based on Maxwell-Garnett mixing rules (solid lines) with simulation results (triangles) for $p = 0.8$ mm.

6.2 Surface Wave Propagation in Perforated Substrates

Building on the results presented above, in this section we turn our attention to a little different problem. We deal with the propagation of surface waves in perforated substrates, since as it has been shown in previous chapter, the relative permittivity of manufacturable structure (ratio $D/p < 1$) can be quite significant and starts between values 3-4.

6.2.1 Surface Waves on Dielectric Slabs

Dielectric slab waveguide is one type of dielectric waveguides in which a wave can propagate without attenuation. The slab is a single layer of homogenous dielectric of certain permittivity ε_{d} (relative permittivity is $\varepsilon_{\mathrm{rd}}$ and relative permeability is assumed to be $\mu_{\mathrm{rd}} = 1$) with height $2h$ surrounded from top and bottom by dielectric regions of smaller relative permittivity (mostly air). In such configuration and under certain conditions, electromagnetic waves can become trapped in between the interfaces due to the total internal reflection and propagate as surface waves of TM and/or TM type. Detailed descriptions based on modal analysis approach or ray tracing methods can be found in e.g. [1, 33, 34]. In here, we only give the most basic theoretical background that is required to determine the properties of perforated dielectrics with respect to surface waves propagation.

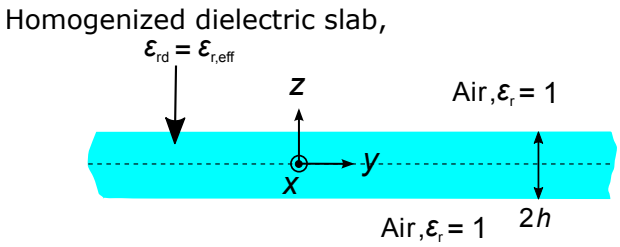

Fig. 6.3: Geometry of the dielectric slab with coordinate system.

The geometry of a general dielectric slab problem is given in Fig. 6.3. Under the assumption that the slab is infinite in the x direction, we can consider the problem to be two-dimensional, allowing no field variation in the x direction. The surface waves are then the waves TE/TM propagating along the slab in the y direction (or $-y$) and can be of two types: even and odd. The type is determined by the symmetry of the magnetic vector potential $\mathbf{A}$, which in this case, has only the $A_y = A$ component. In grounded slab waveguide in which one surface of the slab is covered by a conductor, even TM and odd TE modes do not satisfy boundary conditions and thus are not supported by the structure. In our notation, the coordinate system is somewhat rotated with respect to common notation found in the literature, i.e. we have aligned the extraordinary axis of our geometry with z axis and the direction of propagation along the slab is thus y. Moreover, as our dielectric layer is heterogeneous, we assign it relative permittivity of homogenous equivalent $\varepsilon_{\mathrm{rd}} = \varepsilon_{\mathrm{r,eff}}$ and the propagation constant in homogenized dielectric is indicated as β_d.

By studying the expressions for electric field distribution of surface wave modes on perforated substrates we can arrive at the conclusion, that although the TE waves have only electric field component perpendicular to the axis of perforations, the TM waves have the E-field components perpendicular as well as parallel to the axis of perforations. The permittivity of the material for TE waves should be completely described by ε_o. On the other hand, for TM waves, the permittivity should then lie somewhere between the values ε_e and ε_o.

For the analysis and extraction of the effective permittivity of a perforated slab waveguide, we must define the dispersion relations. The detailed derivation of these formulas can be found in e.g. [1]. The dispersion relations for the TM and TE modes considering dielectric slab with permittivity $\varepsilon_{\mathrm{d}} = \varepsilon_{\mathrm{rd}}\varepsilon_0$ and permeability $\mu_{\mathrm{d}} = \mu_0$ surrounded by air with material properties ε_0, μ_0 are given by:

$$\frac{1}{\varepsilon_{\mathrm{rd}}}\left(\beta_{zd}h\right)\tan\left(\beta_{zd}h\right) = \alpha_{z0}h \quad \text{odd TM}, \tag{6.10}$$

$$\left(\beta_{zd}h\right)\tan\left(\beta_{zd}h\right) = \alpha_{z0}h \quad \text{odd TE}. \tag{6.11}$$

For unattenuated propagation of electromagnetic waves, all the three coefficients: β_{zd}, α_{z0} and β_y must be real. This holds true only if the following relation is satisfied:

$$\beta_0 < \beta_y < \beta_d. \tag{6.12}$$

In our analysis, we consider only the lowest order TE and TM modes, i.e. odd modes TM_0 and TE_0 to examine the behavior of surface waves on anisotropic substrate.

6.2.2 Determining Effective Relative Permittivity from Unit Cell Analysis

Usually, in the analysis and design of dielectric slab waveguides, one is familiar with the height of the slab $2h$ and with its material properties ($\varepsilon_{\mathrm{rd}}$, μ_{rd}) and the cutoff frequencies and propagation constants are to be solved. For this reason, one must solve the transcendent dispersion equations (eq. 6.10 and 6.11). One of the methods to solve such equations is based on graphical numerical technique [34], which allows us to determine all propagating modes and their propagation constants.

For simplicity, in the following text we denote the effective relative permittivity of the slab by $\varepsilon_{\mathrm{rd}}$. The task now is to determine effective ε_{rd} of the perforated slab in TE_0 and TM_0 propagating wave from known propagation constant in the y direction β_y. We obtain β_y from unit cell analysis in eigenmode solver in CST MWS . In unit cell analysis, we proceed similarly like in the case of TEM wave, however, we must add some vertical space above the unit cell.

For TM_0 mode analysis $\varepsilon_{\mathrm{rd}}$ is rewritten in terms of β_{zd} and the final form of the transcendent dispersion equation to be solved numerically is:

$$\frac{\beta_0^2}{\beta_{zd}^2 + \beta_y^2}\left(\beta_{zd}h\right)\tan\left(\beta_{zd}h\right) = \alpha_{z0}h, \tag{6.13}$$

where β_{zd} is our unknown. After obtaining β_{zd} we can calculate $\varepsilon_{\mathrm{rd}}$ for certain mode from modified eq. 6.14

$$\beta_{zd} = \pm\sqrt{\beta_d^2 - \beta_y^2} = \pm\sqrt{\varepsilon_{\mathrm{rd}}\beta_0^2 - \beta_y^2}, \tag{6.14}$$

since $\beta_d = \beta_0\sqrt{\varepsilon_{\mathrm{rd}}}$.

In case of TE_0 mode, we solve eq. 6.15 for β_{zd} and again use eq. 6.16 to obtain $\varepsilon_{\mathrm{rd}}$

$$\beta_{zd}h\tan\left(\beta_{zd}h\right) = \alpha_{z0}h. \tag{6.15}$$

Once the propagation constant βzd is known, the effective relative permittivity for TE_0 mode $\varepsilon_{\mathrm{rd,TE}}$, and for TM_0 mode $\varepsilon_{\mathrm{rd,TM}}$ is then calculated as

$$\varepsilon_{\mathrm{rd}} = \frac{\beta_{zd}^2 + \beta_y^2}{\beta_0^2}. \tag{6.16}$$

6.2.3 Summary

The quasi-static theoretical model based on Maxwell-Garnett mixing rules tends to give useful results even for surface waves on dielectric slabs. As shown in Fig. 6.4 and 6.5, the effective relative permittivity as seen by TE_0 surface wave mode can be approximated with very good agreement by effective permittivity corresponding to polarization perpendicular to axis of perforations. The approximation is valid even for $p = \lambda_0/9.4$ (see Fig. 6.5(right)).

On the other hand, we predicted that the effective relative permittivity seen by propagating TM_0 mode to lie somewhere between the limits given by MG model for parallel and perpendicular polarization, since as has been shown, the TM_0 mode possesses electric field components both with parallel and perpendicular orientation with respect to axis of perforations. In Fig. 6.4(left) and 6.5 (left), we can see the $\varepsilon_{\mathrm{r,eff}}$ to be between the permittivity limits. However, it is interesting that as the frequency goes higher, the permittivity for parallel polarization prevails (see Fig. 6.5(right)).

The discrepancy between the theoretical model and simulation results at 20 GHz for period of perforations $p = 3$ mm and for porosities below circa 60 % (i.e. larger diameter of perforations D) in Fig. 6.4(left) can be assigned to electromagnetic bandgap behavior of the structure. At 20 GHz, the 3 mm period corresponds to electrical length about $\lambda_0/5$ and the effective media concept is no longer accurate.

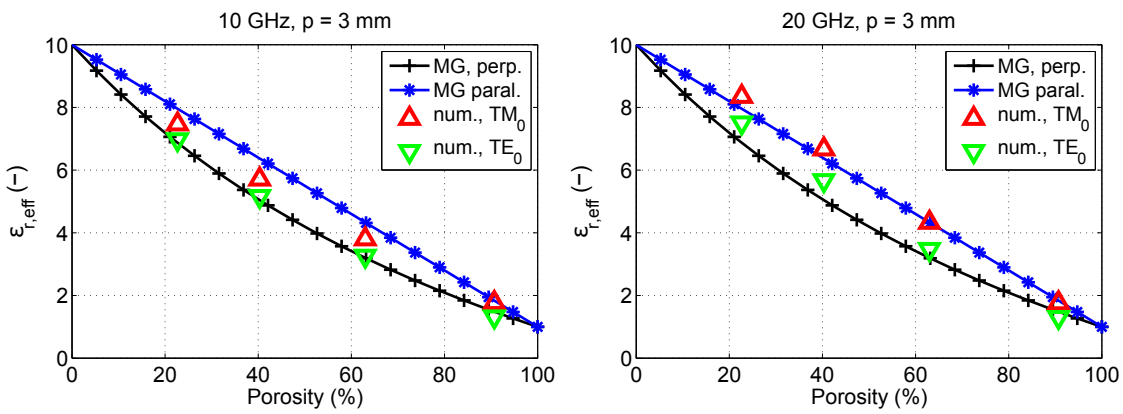

Fig. 6.4: Comparison between analytical and numerical results for period of perforations p =3 mm.

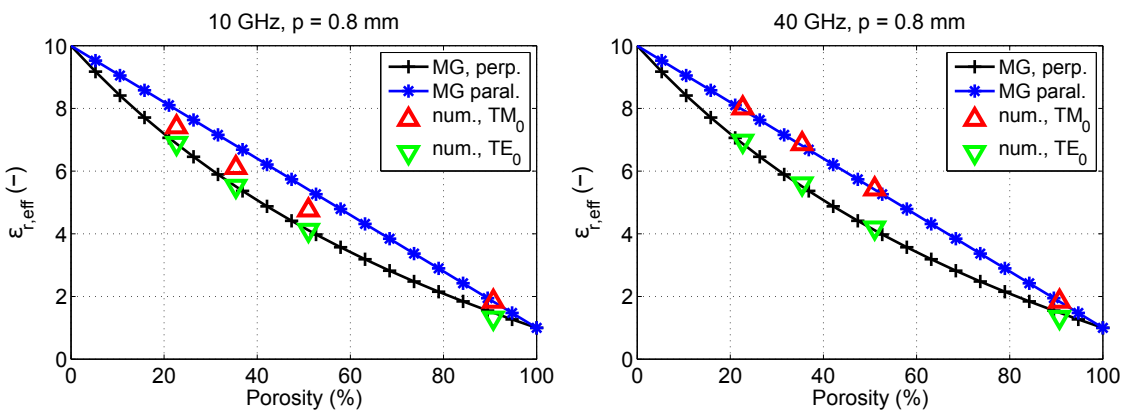

Fig. 6.5: Comparison between analytical and numerical results for period of perforations p =0.8 mm.

Conclusions

The original contributions of the thesis, as pointed out in the Chapter 3, lie in the areas of enhanced gain DRA elements based on the higher-order mode excitation, mutual coupling between HO mode resonators and last but not least, in the area of perforated dielectrics and perforated DRAs.

We have proposed rectangular and cylindrical DRA elements operating with modes TE_{133} and HEM_{133}, respectively. The antennas were configured as simple shaped resonators placed on top of a conductive ground plane. It turned out that the size of the ground plane had non-negligible influence on the maximum achievable gain. We optimized the antennas for maximum gain and we obtained optimum aspect ratios of the basic shapes that maximize the gain. Certain aspect ratios enabled simultaneous excitation of other HO modes thus improving the impedance bandwidth; however, it did not improve the bandwidth of the enhanced gain frequency region. With fabricated prototypes of proposed antennas we have achieved maximum gains of 11.6 dBi for cylindrical and 11.9 dB for rectangular DRAs, revealing about 5.6 dB and 5.9 dB gain improvement compared to fundamental, broadside radiating modes of given resonators.

By introducing a small air gap between the cylindrical resonator and its ground plane, we were able to further increase the gain from 11.6 dBi to 13.2 dBi. The common disadvantage of our HO mode solutions is their limited bandwidth. Even though the resonators were built from material with $\varepsilon_r = 6.15$, the impedance bandwidth was only about 3 %. This bandwidth was extended by excitation of other HO modes in resonator with square footprint; however, the main limitation remained the reduced bandwidth of enhanced gain region.

The concept of cylindrical HEM_{133} mode antenna was utilized for design of mm-wave directive, SIW-fed DRA based on LTCC manufacturing technology at frequency about 26 GHz. Very low losses of the LTCC dielectrics resulted in high radiation efficiency of 87 %. Moreover, due to very good shape accuracy of LTCC technology we obtained excellent agreement between simulations and measurements.

In Chapter 5 we shifted our attention to the evaluation of mutual coupling between rectangular dielectric resonators operating with HO modes intended for gain enhancement. We worked with modes TE_{113}, TE_{115} and finally with the TE_{133}. Resonators excited with TE_{113}, TE_{115} modes turned out to be suitable elements for antenna array applications. Moreover, both modes showed reduced coupling levels compared to fundamental mode DRAs, which makes them interesting for dense array applications. For example TE_{113} mode showed reduced mutual coupling by 12 dB factor in case of separation distance $0.5\lambda_0$ compared to fundamental TE_{111} mode. Excitation of HO mode can thus represent a new mutual coupling reduction technique. Considering TE_{133} mode, due to physical size and the large side-lobes in the E-plane, the element is not suitable for 2D antenna arrays; however, in case of 1D, H-plane antenna arrays, the element gives very similar mutual coupling levels as the fundamental mode DRAs (i.e. TE_{111}).

The third part (Chapter 6) of the thesis is focused on perforated dielectrics and per-

forated DRAs. Analytical model based on quasi-static approximation and on Maxwell-Garnett mixing rules is given and evaluated at microwave frequency bands for TEM wave. Compered to models in the open literature, our model respects the anisotropic properties of the perforated dielectrics and can be directly used to predict properties of perforated dielectrics in various antenna and propagation application areas, e.g. analysis and design of reflectarrays, transmitarrays, planar lenses and other transformation optics devices.

We extend the analysis to propagation of surface waves on perforated substrates. We determined the effective relative permittivities as seen by TM_0 and TE_0 surface wave modes and we successfully used the model derived for TEM wave to pose the limits for TM_0 and TE_0 mode relative permittivities of perforated substrate.

Last, we dealt with the perforated DRAs, we examine the behavior of single element radiators and we verify the usability of effective permittivity models. Resonant frequency shift due to the perforated surrounding of the DRA, instead of air, is investigated as well as the radiation pattern modification caused by edge diffraction of surface waves. We tested the mutual coupling between perforated DRs and we compared the results to conventional DRAs. For porosity of 87 % the mutual coupling increased by only 1 dB factor for perforated DRs $0.5\lambda_0$ apart; however, the increase was almost 5 dB for $1\lambda_0$ separation, which proved that the surface waves in perforated substrate increase the coupling levels among the elements of perforated antenna arrays.

Many interesting areas for a future research open up based on the work presented in this thesis . Considering the HO modes for gain enhancement, important issues are related to extending the bandwidth of the elements. One hint given in Chapter 4 is a controlled excitation of modes TE_{133} and TE_{115} close to each other in the frequency spectrum. Both modes can provide enhanced directivity if the aspect ratio is suitably selected. Another interesting research direction is the excitation of dual linear polarization and eventually circular polarization in such resonators. Hybrid and reconfigurable designs might also be relevant.

In relation to Chapter 5 antenna array design with HO mode elements is very promising. Due to the directive radiation patterns of the single elements, limited use in scanning arrays seems also possible. If working with the TE_{133} mode, we can reduce the size of the array by factor of 4, since the HO mode provides about 6 dB higher gain compared to conventional TE_{111} mode DRA.

The analytical description of perforated dielectrics for permittivity reduction at microwave frequencies seems to be completely lacking in the open literature. Inclusion of the losses into the models deployed in this thesis would be very practical. The perforated dielectrics can be used for design of polarization sensitive devices (each polarization see slightly different relative permittivity). Investigation of different shapes and grids of perforations might also be interesting. Possible gain reduction of perforated DRA and DRA arrays due to surface waves should also be examined.

References

[1] C.A. Balanis. *Advanced Engineering Electromagnetics*. Wiley, 2012. ISBN: 9780470589489.

[2] S. Long, M. McAllister, and Liang Shen. The resonant cylindrical dielectric cavity antenna. *IEEE Transactions on Antennas and Propagation*, 31(3):406–412, May 1983. doi:10.1109/TAP.1983.1143080.

[3] A. Petosa. *Dielectric Resonator Antennas Handbook*. Artech House Antennas and Propagation Library. Artech House Publishers, 2007. ISBN: 978-1596932067.

[4] K. M. Luk and K. W. Leung. *Dielectric Resonator Antennas*. Antennas. Research Studies Press, 2002. ISBN: 978-0863802638.

[5] A. Petosa, S. Thirakoune, and A. Ittipiboon. Higher-order modes in rectangular dras for gain enhancement. In *2009 13th International Symposium on Antenna Technology and Applied Electromagnetics and the Canadian Radio Science Meeting*, pages 1–4, Feb 2009. doi:10.1109/ANTEMURSI.2009.4805098.

[6] A. Petosa and S. Thirakoune. Rectangular dielectric resonator antennas with enhanced gain. *IEEE Transactions on Antennas and Propagation*, 59(4):1385–1389, April 2011. doi:10.1109/TAP.2011.2109690.

[7] D. Guha, A. Banerjee, C. Kumar, and Y. M. M. Antar. Higher order mode excitation for high-gain broadside radiation from cylindrical dielectric resonator antennas. *IEEE Transactions on Antennas and Propagation*, 60(1):71–77, Jan 2012. doi:10.1109/TAP.2011.2167922.

[8] D. Guha, A. Banerjee, C. Kumar, and Y. M. M. Antar. New technique to excite higher-order radiating mode in a cylindrical dielectric resonator antenna. *IEEE Antennas and Wireless Propagation Letters*, 13:15–18, 2014. doi:10.1109/LAWP.2013.2294877.

[9] Kwai-Man Luk, Wai-Kee Leung, and Kwok-Wa Leung. [5] mutual impedance of hemispherical dielectric resonator antennas. *IEEE Transactions on Antennas and Propagation*, 42(12):1652–1654, Dec 1994. doi:10.1109/8.362806.

[10] G. P. Junker, A. A. Kishk, and A. W. Glisson. [6] multiport network description and radiation characteristics of coupled dielectric resonator antennas. *IEEE Transactions on Antennas and Propagation*, 46(3):425–433, Mar 1998. doi:10.1109/8.662662.

[11] R. Chair, A. A. Kishk, and Kai-Fong Lee. [7] comparative study on the mutual coupling between different sized cylindrical dielectric resonators antennas and circular microstrip patch antennas. *IEEE Transactions on Antennas and Propagation*, 53(3):1011–1019, March 2005. doi:10.1109/TAP.2004.842682.

[12] G. D. Loos and Y. M. M. Antar. [10] a new aperture-coupled rectangular dielectric resonator antenna array. *Microwave and Optical Technology Letters*, 7(14):642–644, 1994. URL: `http://dx.doi.org/10.1002/mop.4650071403`, `doi:10.1002/mop.4650071403`.

[13] K. Y. Chow, K. W. Leung, K. M. Luk, and E. K. N. Yung. [11] cylindrical dielectric resonator antenna array. *Electronics Letters*, 31(18):1536–1537, Aug 1995. `doi:10.1049/el:19951080`.

[14] Yong-Xin Guo, Kwai-Man Luk, and Kwok-Wa Leung. [13] mutual coupling between millimeter-wave dielectric-resonator antennas. *IEEE Transactions on Microwave Theory and Techniques*, 47(11):2164–2166, Nov 1999. `doi:10.1109/22.798016`.

[15] J. S. Colburn and Y. Rahmat-Samii. Patch antennas on externally perforated high dielectric constant substrates. *IEEE Transactions on Antennas and Propagation*, 47(12):1785–1794, Dec 1999. `doi:10.1109/8.817654`.

[16] A. Patrovsky and Ke Wu. Substrate integrated image guide (siig) - a low-loss waveguide for millimetre-wave applications. In *2005 European Microwave Conference*, volume 2, pages 4 pp.–, Oct 2005. `doi:10.1109/EUMC.2005.1610071`.

[17] A. Patrovsky and Ke Wu. Substrate integrated image guide (siig)-a planar dielectric waveguide technology for millimeter-wave applications. *IEEE Transactions on Microwave Theory and Techniques*, 54(6):2872–2879, June 2006.

[18] J. B. Muldavin and G. M. Rebeiz. Millimeter-wave tapered-slot antennas on synthesized low permittivity substrates. *IEEE Transactions on Antennas and Propagation*, 47(8):1276–1280, Aug 1999. `doi:10.1109/8.791943`.

[19] A. Patrovsky and K. Wu. 94-ghz planar dielectric rod antenna with substrate integrated image guide (siig) feeding. *IEEE Antennas and Wireless Propagation Letters*, 5(1):435–437, Dec 2006. `doi:10.1109/LAWP.2006.885014`.

[20] A. Patrovsky and K. Wu. Substrate integrated image guide array antenna for the upper millimeter-wave spectrum. *IEEE Transactions on Antennas and Propagation*, 55(11):2994–3001, Nov 2007. `doi:10.1109/TAP.2007.908558`.

[21] A. Petosa, A. Ittipiboon, and S. Thirakoune. Perforated dielectric resonator antennas. *Electronics Letters*, 38(24):1493–1495, Nov 2002. `doi:10.1049/el:20021074`.

[22] A. Petosa, S. Thirakoune, and A. Ittipiboon. Array of perforated dielectric resonator antennas. In *IEEE Antennas and Propagation Society Symposium, 2004.*, volume 1, pages 1106–1109 Vol.1, June 2004. `doi:10.1109/APS.2004.1329868`.

[23] A. Petosa, S. Thirakounc, M. Zuliani, and A. Ittipiboon. Comparison between planar arrays of perforated dras and microstrip patches. In *2005 IEEE Antennas and Propagation Society International Symposium*, volume 2A, pages 168–175 vol. 2A, July 2005. `doi:10.1109/APS.2005.1551764`.

[24] S. H. Zainud-Deen, S. M. Gaberand, and K. H. Awadalla. Transmitarray using perforated dielectric material for wideband applications. *Progress In Electromagnetics Research M*, 24:1–13, 2012. `doi:10.2528/PIERM12020110`.

[25] A. Petosa, A. Ittipiboon, and S. Thirakoune. Investigation on arrays of perforated dielectric fresnel lenses. *IEE Proceedings - Microwaves, Antennas and Propagation*, 153(3):270–276, June 2006. doi:10.1049/ip-map:2005019.

[26] C. S. Lee, S. W. Lee, R. Davis, and J. Tsui. Perforated dielectric lens. *Microwave and Optical Technology Letters*, 5(2):92–94, Feb 1992. doi:10.1002/mop.4650050214.

[27] A. E. Mahmoud, W. Hong, Y. Zhang, and A. Kishk. W-band mutlilayer perforated dielectric substrate lens. *IEEE Antennas and Wireless Propagation Letters*, 13:734–737, 2014. doi:10.1109/LAWP.2014.2316144.

[28] M. Mrnka and Z. Raida. Linearly polarized high gain rectangular dielectric resonator antenna. In *2016 10th European Conference on Antennas and Propagation (EuCAP)*, pages 1–4, April 2016. doi:10.1109/EuCAP.2016.7481588.

[29] A. Dadgarpour, B. Zarghooni, B. S. Virdee, T. A. Denidni, and A. A. Kishk. Mutual coupling reduction in dielectric resonator antennas using metasurface shield for 60-ghz mimo systems. *IEEE Antennas and Wireless Propagation Letters*, 16:477–480, 2017. doi:10.1109/LAWP.2016.2585127.

[30] CH. Kittel. *Introduction to Solid State Physics, 8e.* Wiley, 2004. ISBN: 978-0-471-41526-8.

[31] A. H. Sihvola and J. A. Kong. Effective permittivity of dielectric mixtures. *IEEE Transactions on Geoscience and Remote Sensing*, 26(4):420–429, July 1988. doi:10.1109/36.3045.

[32] M. Born and E. Wolf. *Principles of Optics: Electromagnetic Theory of Propagation, Interference and Diffraction of Light, 7e.* Cambridge University Press, 1999. ISBN: 9780521642224.

[33] R.F. Harrington. *Time Harmonic Electromagnetic Fields.* Wiley-IEEE Press, 2001. ISBN: 978-0-471-20806-8.

[34] R.E. Collin. *Field Theory of Guided Waves, 2e.* Wiley-IEEE Press, 1990. ISBN: 978-0-87942-237-0.

Michal Mrnka

Poznaňská 2
616 00 Brno
Czech Republic

e-mail: xmrnka@gmail.com
Phone 1: +420 776 498 767
Phone 2: +421 948 046 957

Education

2013 - current **Brno University of Technology** - Brno, Czech Republic
Ph.D. in Radio electronics.
Research Topic: Higher-order modes in dielectric resonator antennas, perforated dielectrics

2010-2013 **Brno University of Technology** - Brno, Czech Republic
MSc, Electronics and Communication.
Graduated summa cum laude

2010-2011 **Tampere University of Technology** - Tampere, Finland
Erasmus exchange student (2 semesters)

2007-2010 **Brno University of Technology** - Brno, Czech Republic
BSc, Electronics and Communication.

Working experience and research stays

2015-current **ERA a.s.** - Pardubice, Czech Republic
R&D Antenna engineer.
Fields: Antenna design for VHF and L band radars, antenna placement modelling, radar cross section analysis

10/2015 **Technical University of Kosice** - Košice, Slovakia
Visiting PhD student.
Topic: Low Temperature Co-Fired Ceramic (LTCC) based dielectric resonator antennas for millimeter wave applications.

11/2014 **Graz University of Technology** - Graz, Austria
Visiting PhD student.
Topic: Wide-band dielectric resonator antennas for energy harvesting applications

09/2013 to 07/2014	**Max Planck Institute for Radio Astronomy** - Bonn, Germany Intern with microwave technology group. Topics: Microwave measurements, LabVIEW programming, development of waveguide components for Ka band
02/2012 to 08/2013	**ERA a.s.** - Pardubice, Czech Republic Master Thesis internship. Topic: Design of a range illuminating antenna in L-band, preparation of the technical documentation and performance verification by measurements.
08/2011 to 05/2013	**FEI Company** - Brno, Czech Republic Electronics intern. Topics: PCB layouting, simple circuits design, electronic measurements, technical support of the development group.

Industrial, basic and applied research projects

2014 -2016	**Mm-wave electromagnetic structures for biomedical research** Czech Grant Agency project GACR P102/12/1274 Reconfigurable hybrid dielectric resonator antennas and directive dielectric resonator antennas for on-body and off-body communications.
2015 -2016	**Wireless Power Transmission for Sustainable Electronics** European Project COST WiPE IC1301 Antennas for energy harvesting, Low Temperature Co-Fired Ceramic materials for efficient millimeter-wave dielectric resonator antennas.
9/2015 to 3/2016	**Volkswagen** - Industrial project Development of a methodology for in-car electromagnetic field modeling.
1/2015 to 6/2015	**Antenna Toolbox for MATLAB** Technological Agency of Czech Republic project TA04010457 Cooperation on 1D Method of Moments implementation for wire antennas.

Awards

06/2013 **Dean's award for Master's thesis**
Topic: Transmitting Antenna With Dual Circular Polarization For Indoor Antenna Measurement Range

06/2010 **Dean's award for Master's thesis**
Topic: Study of Gel Electrolytes by Magnetic Resonance Methods

Languages

English
Fluent (C1)
German
Intermediate (A2)

Software skills

CST, HFSS, MATLAB, Ansys, Comsol, AWR Microwave Office, Ansoft Designer, Agilent EMpro, PSpice, DxDesigner, PADS, LabVIEW, Microsoft Office etc.

Additional education

08/2016 **Antenna Arrays and Reflectarrays**
course within the European School of Antennas framework, Catholic University of Leuven, Belgium

07/2015 **Antenna Imaging Techniques**
course within the European School of Antennas framework, Delft University of Technology, The Netherlands

07/2014 **Summer school on Microwaves and Lightwaves**
Technical University of Denmark

09/2012 **Summer school on Nanotechnology**
Ege University and Izmir Institute of Technology, Turkey

07/2011 **Summer school on Radar/SAR**
Fraunhofer Institute for High Frequency Physics and Radar Techniques FHR in Bonn, Germany

Abstract

The thesis deals with the excitation of higher-order modes in the rectangular and cylindrical dielectric resonator antennas for gain enhancement purpose. The properties and limitations of the antenna elements are studied numerically. Mutual coupling between the higher-order mode dielectric resonators is examined and the results prove the elements to be suitable for antenna array applications. For perforated dielectrics, an analytical model of effective permittivity that respects its anisotropic properties is proposed. The model is based on the Maxwell Garnett approximation of inhomogeneous media. Surface waves on perforated substrates are then studied and the validity of the analytical model is verified also in this case. The dielectric resonator antennas embedded in perforated substrates are studied and certain degradations in antenna properties are pointed out.